

# A new method for the separation of paramagnetic and ferromagnetic susceptibility anisotropy using low field and high field methods

Paul R. Kelso,<sup>1</sup> Basil Tikoff,<sup>2</sup> Mike Jackson<sup>3</sup> and W. Sun<sup>3</sup>

<sup>1</sup>Department of Geology and Physics, Lake Superior State University, 650 W. Easterday Ave., Sault Ste. Marie, MI 49783. E-mail: pkelso@lssu.edu

<sup>2</sup>Department of Geology and Geophysics, University of Wisconsin-Madison, Madison WI 53706

<sup>3</sup>Institute for Rock Magnetism and Department of Geology and Geophysics, University of Minnesota, Minneapolis, Minnesota 55455

Accepted 26 March 2002. Received 19 March 2002; in original form 18 June 2001

## SUMMARY

Most rocks contain both ferromagnetic and paramagnetic minerals that contribute to their bulk magnetic susceptibility and the anisotropy of magnetic susceptibility. Anisotropy of magnetic susceptibility techniques typically measure the net susceptibility and are not able to separate paramagnetic and ferromagnetic contributions. Since different minerals may form at various times and/or under different conditions, examination of their individual contributions provides unique information related to the rock's formation and evolution. By subjecting a sample to high magnetic fields, the ferromagnetic minerals become saturated and the contribution of the paramagnetic minerals can be evaluated (the slope of the line at high field values, on a field vs magnetization plot). Using this approach, we developed a new technique that separates the ferromagnetic and paramagnetic components of standard 1 inch cylindrical samples using a Vibrating Sample Magnetometer. This separation is tested by artificially combining separate samples with known paramagnetic-only and ferromagnetic-only behaviour. By comparing the high-field results of a combined paramagnetic and ferromagnetic signal to the classic low field alternating current susceptibility of the paramagnetic-only signal, we demonstrate that the high field anisotropy is the result solely of the paramagnetic fabric even when the low field anisotropy of magnetic susceptibility is dominated by the ferromagnetic minerals. A ferromagnetic-only fabric is calculated for the combined paramagnetic and ferromagnetic rock, by tensor subtraction of the high field (paramagnetic-only) and low field (paramagnetic plus ferromagnetic) measurements on the same sample. Application of this technique to natural samples of combined paramagnetic and ferromagnetic behaviour is discussed.

**Key words:** anisotropy, magnetic susceptibility, magnetite, paramagnetism.

## INTRODUCTION

Pioneering work using magnetic methods to characterize the preferred orientation of minerals within rock samples occurred during the 1940's and 1950's (Ising 1943; Graham 1954), but only over the past 20 yr has the anisotropy of magnetic susceptibility (AMS) gained widespread use to examine the fabric of sedimentary, igneous and metamorphic rocks (reviews by Jackson & Tauxe 1991; Rochette *et al.* 1992; Tarling & Hrouda 1993; Borradaile & Henry 1997). AMS is typically measured in a low field (<0.5 mT), with an alternating current, magnetic induction bridge (Jelinek 1973; Collinson 1983; Tarling & Hrouda 1993). The AMS is a result of a combination of shape orientation, distribution anisotropy and crystallographic orientation (e.g. Borradaile & Henry 1997).

Minerals have magnetic susceptibilities that are diamagnetic (magnetization decreases linearly with increasing field), paramagnetic (magnetization increases linearly with increasing field), or fer-

romagnetic (*sensu lato*; magnetization increases nonlinearly with increasing field) (e.g. Dunlop & Özdemir 1997). Paramagnetic and ferromagnetic susceptibilities are typically much greater than diamagnetic susceptibility and are thus the focus of this study. AMS represents a summation of the anisotropic susceptibilities of all the mineral grains within a sample. Thus, AMS depends not only on the degree of alignment of these particles, but also on their intrinsic anisotropies and susceptibility magnitude. When multiple phases make significant contributions to a rock's total susceptibility, the AMS is strongly dependent on the relative abundance of the different minerals.

As a result of these difficulties, the interpretation of magnetic fabrics is generally limited to rocks in which the magnetic susceptibility is dominated by a single mineral. The interpretation of samples with contributions from multiple phases often requires the implicit assumption that different minerals have similarly oriented AMS ellipsoids. Alternatively, one can devise a method for separation of the magnetic components.

There are generally four methods recognized for the separation of paramagnetic and ferromagnetic minerals: (1) A mathematical method based on site analysis (Henry & Daly 1983; Henry 1985); (2) Measurement of the anisotropy of remanence (McCabe *et al.* 1985; Jackson 1991; Hrouda 2002); (3) Utilizing the temperature dependence of susceptibility (Richter & van der Pluijm 1994); and (4) Utilizing the field dependence of susceptibility (Owens & Bamford 1976; Rochette & Fillion 1988; Hrouda & Jelínek 1990; Bergmüller & Heller 1996; Martín-Hernández & Hirt 2001). Method 1 is based on a statistical analysis of multiple cores, and assumes that the variation in susceptibility is a function solely of ferromagnetic mineral content. Method 2 only measures contributions of the ferromagnetic minerals and consequently is strongly affected by variations in mineral grain size, domain state, applied field and oxidation state of these minerals. It is difficult to directly compare remanence and the susceptibility anisotropy ratio because they are often different for measurements on the same sample (Jackson 1991; Collombat *et al.* 1993). In addition, ferromagnetic minerals generally form less than 1 volume percent of the rock, and are often more strongly affected by diagenesis, retrogression, and oxidation than paramagnetic minerals and therefore are more likely to be the result of secondary processes. Method 3 requires assumptions about the temperature dependence of magnetic susceptibility. Although paramagnetic materials follow the Curie–Weiss Law, the temperature dependence of ferromagnetic minerals is not as predictable (e.g. Moskowitz *et al.* 1997). Ferromagnetic minerals have been modelled both as temperature independent (Hrouda 1994; Richter & van der Pluijm 1994) and varying linearly with temperature (Hrouda *et al.* 1997), but in many cases neither of these is applicable. Also, it should be noted that for method 3, antiferromagnetic, weak paramagnetic and diamagnetic materials do not follow the Curie–Weiss Law and thus are often grouped with the ferromagnetic component (Rochette 1994).

Method 4 is based on the field dependence of susceptibility and relies on the different response of ferromagnetic and paramagnetic minerals to large applied fields, i.e. >300 mT (Fig. 1). With an increase in applied field ( $H$ ), the magnetization ( $M$ ) for paramagnetic and diamagnetic minerals increases and decreases, respectively, in a linear manner (Fig. 1a). In contrast, ferromagnetic minerals tend to saturate ( $M_s$ ) at some applied field ( $H_s$ ), such that there is no longer an increase in magnetization with increasing applied field (Fig. 1b). Consequently, for rocks that have both ferromagnetic and paramagnetic minerals, changes in magnetization at fields greater than ferromagnetic saturation, ( $H_s$ ), are due primarily to the paramagnetic susceptibility ( $\kappa$  in Fig. 1c). The high-field AMS (HFAMS) ellipsoid is determined by measuring the high field slope in a num-

ber of directions (6–24) and then calculating the magnitude and direction of the principal axes of the HFAMS ellipsoid, similar to calculation of the low-field AMS (LFAMS) ellipsoid (Jelínek 1973; Collinson 1983; Tarling & Hrouda 1993). Note that in the maximum fields present in this study ( $\sim 500$  mT) antiferromagnetic minerals and high coercivity ferrimagnetic minerals are unlikely to saturate and thus the high field susceptibility would contain a contribution from these minerals along with a small contribution ( $\sim 10^{-5}$  SI) from any diamagnetic minerals present. It is important to characterize the magnetic mineralogy of a sample so that contributions to high field susceptibility from sources other than paramagnetic minerals are recognized.

Measurements of high field anisotropy have been made using a torque magnetometer (Banerjee & Stacey 1967; Kadzialko-Hofmkl 1986; Parma 1988; Hrouda & Jelínek 1990; Folami & Hailwood 1991; Aubourg *et al.* 1995; Bergmüller & Heller 1996; Martín-Hernández & Hirt 2001) or a high field, rotating sample, cryogenic magnetometer Rochette & Fillion (1988); Aubourg *et al.* (1995). Although these techniques have great potential to separate paramagnetic and ferromagnetic fabrics, torque magnetometers and high-field cryogenic magnetometers are not available in most magnetic laboratories and HFAMS is not routinely applied. These methods, however, are not as sensitive to geometric effects and field inhomogeneity as the HFAMS technique described in this paper.

We have developed a new experimental set-up using a vibrating sample magnetometer, Princeton Measurements Corp. model 3900, to separate the high field paramagnetic component of AMS from the ferromagnetic component of both natural and natural/synthetic samples. We first apply the technique to samples dominated by paramagnetic susceptibility, and compare the high field, direct current AMS to the more commonly measured low field, alternating current AMS. The technique is also applied to samples with a known paramagnetic fabric plus a known ferromagnetic fabric, and we show that it successfully separates the component fabrics. The application of the technique is limited to samples with easily saturated ferromagnetic minerals, e.g. magnetite, because the peak applied field with this VSM is limited to 0.5–1.0 T depending on pole piece separation (100 mm–25 mm respectively) and, thus, on sample size.

## CHARACTERIZATION OF THE THOMSON FORMATION

For our samples, we chose the Thomson Formation of northern Minnesota. We chose this rock type because previous work (Johns *et al.* 1992; Sun *et al.* 1995) had shown that parts of the Thomson Formation contained primarily a paramagnetic signal. We used this

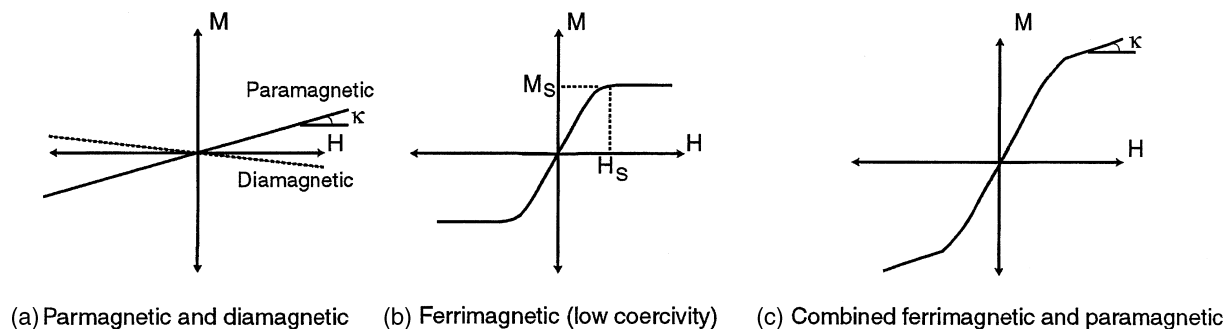


**Figure 1.** Schematic hysteresis loops for different types of magnetic material where  $H$  is the applied magnetic field,  $H_s$  the saturating field,  $M$  the sample magnetization,  $M_s$  the saturation magnetization and  $\kappa$  the paramagnetic susceptibility: (a) diamagnetic and paramagnetic material; (b) low coercivity ferromagnetic material; (c) combined paramagnetic and ferromagnetic material.

absence of a significant ferromagnetic signal to test whether the high field method was able to separate the natural paramagnetic signal and an added ferromagnetic component of known magnitude and intensity. Below we describe the pertinent magnetic characteristics of the Thomson Formation, in order to constrain our high-field experiments.

The Thomson Formation is a middle Proterozoic sequence of metagreywackes and slates deposited as part of the Animikie Group in a foreland basin of the Penokean Orogeny (Southwick *et al.* 1988; Holst 1984). The slates and metagreywackes in the study area were deposited as turbidites. The coarser-grained greywacke layers contain detrital quartz and feldspar grains, with accessory metamorphic phyllosilicates. The finer-grained slates are composed primarily of phyllosilicates, including both detrital and metamorphic grains (Morey 1983b). The study area was deformed and metamorphosed during the Penokean Orogeny, approximately 1.9–1.83 Ga (Van Schmus 1976, 1980; Sims *et al.* 1989).

Previous magnetic studies on the Thomson Formation (Johns *et al.* 1992; Sun *et al.* 1995) found AMS fabrics were dominantly oblate, with a strong foliation and weak lineation. A subset of the specimens studied by Sun *et al.* (1995) were used for our study. Sun *et al.* (1995) also calculated March strains for chlorite in selected specimens, using X-ray texture goniometer data. Their results show a close match between the principal axis orientations of AMS and March strain, where the fabric is oblate and the minimum direction is perpendicular to the foliation, which is consistent with an AMS dominated by the paramagnetic chlorites.

Hysteresis loops measured on Thomson Formation samples at room temperature are essentially straight lines through the origin with positive slopes, indicating that paramagnetic minerals dominate the magnetic signature (Fig. 2). The magnetic susceptibility contributions of paramagnetic versus ferromagnetic minerals for the Thomson Formation samples were evaluated via measurements of magnetic properties as a function of temperature (20–300 K) and applied field (0–2.5 T) with a Quantum Designs MPMS2 (Fig. 3). For temperatures above 50° K, the susceptibility is almost entirely the result of paramagnetic minerals.

X-ray diffraction measurements suggest that the most common silicates are the chlorite-group minerals clinocllore and chamosite (Sun *et al.* 1995). These minerals are structurally similar trioctahedral chlorites, clinocllore is the Mg-rich species and chamosite is the Fe-rich species (Deer *et al.* 1966; Bailey 1988). Borradaile *et al.* (1987) found that for four types of chlorite (diabantite-ripidolite, leuchtenbergite, thuringite, and an unnamed variety), the mean

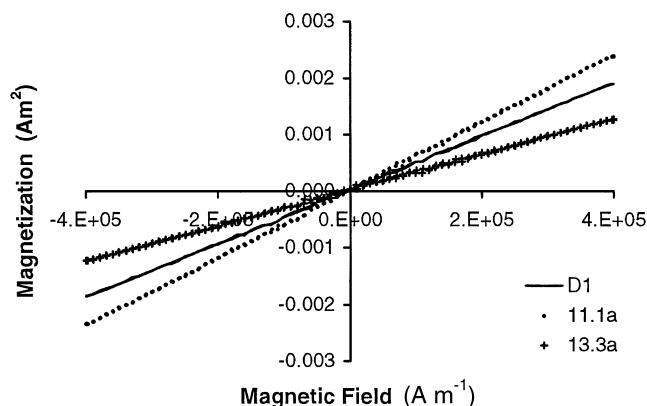


Figure 2. Room temperature hysteresis loops for three representative Thomson Formation samples.

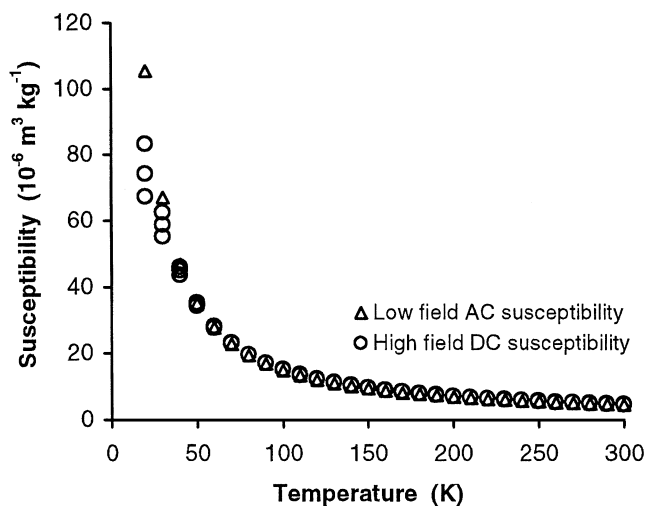


Figure 3. Measurements of susceptibility as a function of temperature for low field (0.0003 T), alternating current and high field (1–2.5 T) direct current on a 256 mg sample from core D of the Thomson Formation. The approximate  $1/X$  temperature dependence of susceptibility is consistent with paramagnetic minerals dominating the room temperature susceptibility. The high field susceptibility is plotted for three field intervals, 1.0–1.5, 1.5–2.0, 2.0–2.5 T, at each temperature, but above 50 K there is no measurable variation in susceptibility with field. The multiple values of high field susceptibility below 50 K are due to nonlinearity between 1.0 and 2.5 T, resulting from incomplete ferromagnetic saturation and/or paramagnetic approach to saturation.

susceptibilities ranged from  $0.7 \times 10^{-4}$  to  $15.5 \times 10^{-4}$  SI, and anisotropies ( $K_{\max}/K_{\min}$ ) ranged from 1.15 to 1.75. For other chlorites, such data have not been published, but some of the properties can be estimated from their chemical composition (e.g. Collinson 1983). For clinocllore and chamosite, Hrouda (1987) has estimated respective susceptibilities of  $5 \times 10^{-4}$  and  $28 \times 10^{-4}$  SI. These values are consistent with the observed mean susceptibilities for our samples (Table 1).

## EXPERIMENTAL DESIGN FOR HIGH FIELD AMS

### Equipment

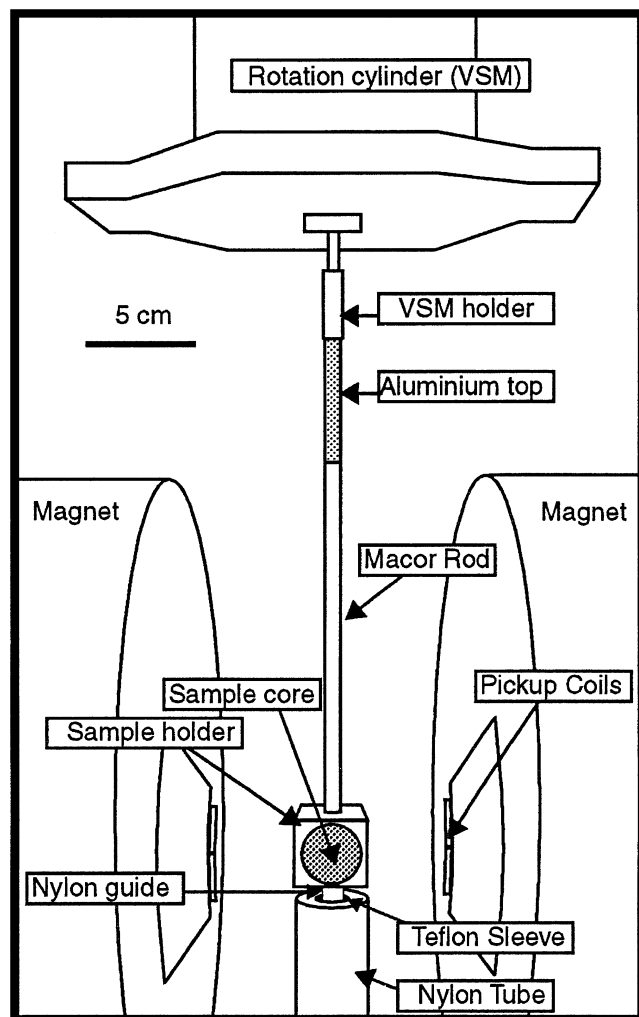
High field AMS measurements were made with a Princeton Measurements Vibrating Sample Magnetometer (VSM) at the Institute for Rock Magnetism at the University of Minnesota. The electromagnet of this VSM is capable of producing applied fields up to 2.2 T depending on applied current and the separation distance between the pole pieces. The maximum applied field decreases as the magnet pole separation increases. The Thomson Formation samples were standard 25 mm diameter by 22 mm high cores. Thus, the minimum possible pole spacing is approximately 40 mm to allow the corners of the sample to fit through the poles during a rotation, when the long axis of the core was oriented horizontally. In order to minimize sample shape effects (see below), we used a pole piece spacing of 97 mm for all HFAMS measurements in this study. The maximum applied field in this configuration is approximately 500 mT.

Samples are centred in a nylon cubic sample holder with a 25.4 mm hole drilled in the centre. The sample holder is attached to a Macor rod suspended from the vibrating sample head. The bottom of the sample holder has a nylon rod that extends down into a teflon-lined nylon tube (Fig. 4). The purpose of the rod on the bottom of the

**Table 1.** Magnetic susceptibility of individual Thomson Formation only samples measured at low field with a Kappa bridge and at high field by calculating the slope of the highest 8 per cent of the applied field vs. magnetization loops on the VSM.

Sample number	Low field susceptibility (Kappa Bridge)						High field susceptibility (VSM)							
	$K_{\min}$ SI ( $10^{-6}$ )	$K_{\text{int}}$ SI ( $10^{-6}$ )	$K_{\max}$ SI ( $10^{-6}$ )	$K_{\min}$ Dec.	$K_{\min}$ Inc.	$K_{\max}$ Dec.	$K_{\max}$ Inc.	$K_{\min}$ SI ( $10^{-6}$ )	$K_{\text{int}}$ SI ( $10^{-6}$ )	$K_{\max}$ SI ( $10^{-6}$ )	$K_{\min}$ Dec.	$K_{\min}$ Inc.	$K_{\max}$ Dec.	$K_{\max}$ Inc.
C1	486	581	587	197	1	289	65	447	554	563	200	3	296	61
D1	479	570	574	173	18	265	6	448	556	577	173	15	284	54
11.1a	478	575	583	219	86	359	3	454	554	567	27	88	164	2
11.2	479	577	582	224	86	1	3	461	554	566	290	86	190	0
11.4b	461	557	565	214	86	352	3	430	539	549	264	86	110	3
11.6	462	559	565	202	86	352	3	431	540	544	14	85	176	5
11.7	463	560	567	205	85	2	4	438	541	548	315	86	185	3
13.1b	255	282	295	309	71	183	11	232	268	284	221	79	20	11
13.2a	256	283	295	292	73	181	6	233	257	274	237	74	18	13
13.3a	265	293	308	295	71	175	10	252	281	300	231	68	0	14
13.3b	256	283	297	296	70	175	10	232	260	278	242	78	6	6
13.5b	266	292	309	307	68	175	15	251	263	298	266	66	3	3
Magnetite disc 1*	733	1381	1422	261	86	9	1							
Magnetite disc 2*	451	602	823	243	43	46	46							
MnO <sub>2</sub> standard	697.5	698.2	699.2	270	77	90	13							

Magnetic susceptibilities along the principal directions are  $K_{\min}$ —minimum,  $K_{\text{int}}$ —intermediate,  $K_{\max}$ —maximum, Dec.—Declination and Inc.—Inclination. \*The magnetic susceptibility was normalized by a sample volume of  $10 \text{ cm}^3$ .

**Figure 4.** Diagram of VSM set up to measure high field AMS.

sample holder is to ensure that the sample remains precisely centred when the sample rotates into different orientations. If the sample does not remain centred the result can be a variation of the signal which appears similar to AMS, but is a result of slight changes in the positioning of the sample.

#### Geometric effects

Instruments typically used for LFAMS measurements are fairly insensitive to variations in sample positioning, whereas the VSM measures a signal that varies significantly with small displacements of the sample, or changes in sample shape or size. Consequently, it was essential to carefully consider geometric effects related to the spatial variation in VSM sensitivity, i.e. the instrumental response function. For an infinitesimal sample, the measured dipole moment is accurate when the sample is precisely centred in the measurement space. A displacement of the point magnetic dipole along the applied field axis toward one of the pickup coil sets results in erroneously large measured values (Fig. 5). A displacement of the point magnetic dipole perpendicular to this axis produces lower moment determinations (Fig. 5). As any real sample of finite extent is an assemblage of off-centred infinitesimal magnetic dipoles, the measured magnetic moment is the sum of the instrument responses to each of these elementary eccentric dipoles. The measured moment depends on both the sample magnetization and how the sample occupies space in the magnetometer. Alternatively stated, the measured magnetic moment is the convolution of the instrumental response function with the spatial variation in magnetization of the sample.

Anisotropy determination requires measurements in different orientations ( $\theta$ ). Directional variability in magnetic properties measured with a VSM can be produced by at least three effects: anisotropy, heterogeneity within the sample, and sample shape. Isolation of the anisotropy signal requires recognition of, and correction for, shape and heterogeneity effects. A brief description of these two effects is given below and a more detailed analysis is presented in Appendix A.

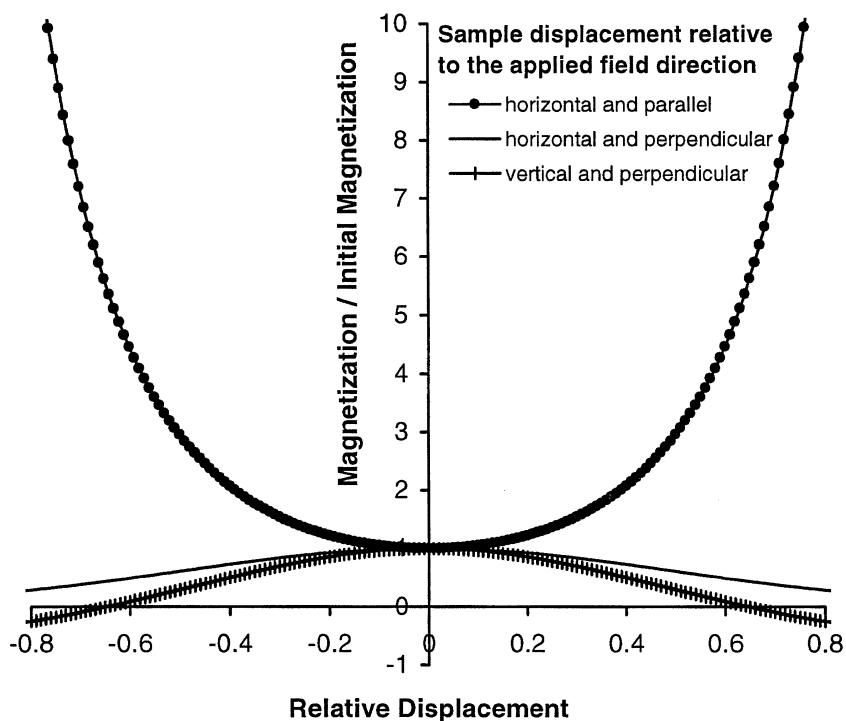


**Figure 5.** Calculated variation in signal strength with position for a point magnetic dipole of constant moment  $m_0$ , where  $Z$  is vertical displacement,  $Y$  is displacement horizontal and parallel to the coil axis and  $X$  is displacement horizontal and perpendicular to the coil axis. Displacements from the centre of the measurement space are normalized by half the pole gap ( $d$ ); the scale thus ranges from 0 (perfectly centred) to 1 (at the pole face) in the  $y$  direction. The pole gap is 2.5 times the pickup coil diameter for these calculations.

Sample shape effects are due to portions of the sample (e.g. corners, edges etc.) moving toward and away from the VSM sensor coils when the sample is rotated into different orientations. The effect of sample shape was quantified by measuring a 25 mm cylinder filled with  $\text{MnO}_2$  powder. The  $\text{MnO}_2$  was glued in place with low-viscosity super glue and endcaps were glued onto the cylinder.  $\text{MnO}_2$  was chosen for the standard because it is isotropic and has a bulk paramagnetic magnetic susceptibility similar to that of our natural samples (as determined by hysteresis loops). The  $\text{MnO}_2$  standard measured with the low-field KLY-2 Kappa bridge had an AMS of less than 0.3 per cent. When rotated parallel to the core axis in the VSM, shape effects are small and the standard had an apparent anisotropy of approximately 1 per cent, even at a pole separation of 51 mm (Fig. 6). This suggests that the sample remains well centred during rotation and that this small apparent anisotropy was likely due to slight variations in sample position and effects from the corners of the sample holder. However, when the  $\text{MnO}_2$  standard was rotated perpendicular to the core axis in the VSM, the standard had a significant apparent anisotropy due to the shape effect, consistent with the quantitative model in Appendix A. With a pole spacing of 51 mm, the apparent anisotropy had strong  $\sin(2\theta)$  (length/diameter) and  $\sin(4\theta)$  (corner) components. The  $\sin(2\theta)$  term, which could be mistaken for an AMS, amounted to approximately 10 per cent apparent anisotropy. Shape effects were much weaker at a pole separation of 97 mm, with apparent anisotropy of <3 per cent (Fig. 6). For this reason, we used the wider pole spacing in all HFAMS determinations. The effect of sample shape was removed from our results via a method described in Appendix B.

Heterogeneity affects HFAMS measurements through the varying VSM response resulting from concentrations of more highly or weakly magnetic material in different parts of the sample. The effects of sample heterogeneity can not be isolated from the suscep-

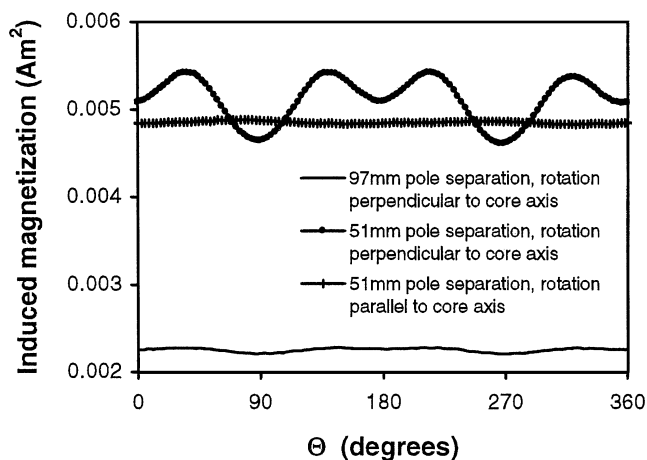


**Figure 6.** The induced magnetization vs. orientation ( $\theta$ ) for the  $\text{MnO}_2$  standard rotated parallel to the core axis for a pole spacing of 51 mm and perpendicular to the core axis or pole spacings of 51 and 97 mm (the pole spacing used in this study). The approximately 1 per cent variation in magnetization when rotated parallel to the core axis is likely due to slight variations in the sample position and contributions from the sample holder. Due to sample shape there is a variation in the observed magnetization of 16 per cent for a 51 mm pole spacing and 3 per cent for a 97 mm pole spacing. The reason for the offset of the curves is that different peak applied fields were used for the 51 and 97 mm pole spacing, i.e. a 700 mT and 300 mT applied field respectively.

tibility anisotropy, and we anticipate that in coarse-grained igneous rocks, or in strongly stratified materials, heterogeneity will probably represent the greatest source of error in high-field anisotropy measurements using a VSM.

### High field AMS measurements

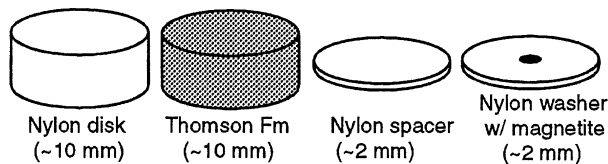
Hysteresis loops were measured in multiple orientations as the sample holder was rotated successively around its  $X$ ,  $Y$  and  $Z$  axes; where the core axis is  $Z$  in sample coordinates and  $X$  is defined as north. The hysteresis loop configuration was: (1) 500 mT maximum field; (2) 12.6 mT field increment between measurements; (3) 0.5 s averaging time for each measurement; and (4) 45° rotation increment between loops. Since the sample was rotated around 3 axes at 45° intervals, 24 hysteresis loops were measured on each sample. Consequently, each orientation was measured at least twice (i.e. in the positive and negative direction), and there were four independent measurements taken along each axis. Individual hysteresis loops required about two minutes and the complete suite of measurements for an individual sample took 50–60 min.

The software for analysing this data is outlined in Appendix B. The first programme calculated the high field slope of the line, using the highest field values, 400–500 mT for this study. The second programme accounted for the geometric effects, normalized susceptibilities between the different rotations using the common positions, and produced a series of 12 independent values of high field magnetic susceptibility. The eigen quantities from these data were calculated using the same software that processes the LFAMS data. A discussion of the HFAMS calculation and an associated errors analysis are contained in Appendix C.

### Sample preparation

Initially LFAMS was measured on 14 Thomson Formation cores with the KLY-2 Kappa Bridge. Six of the samples were cut through the centre, perpendicular to the core axis with a rock saw prior to AMS measurements. A ~2 mm thick nylon spacer was inserted into these samples to maintain their length–height ratios during AMS measurements (Fig. 7). High-field measurements were then made on all 14 samples.

### Components



### Experimental Setup

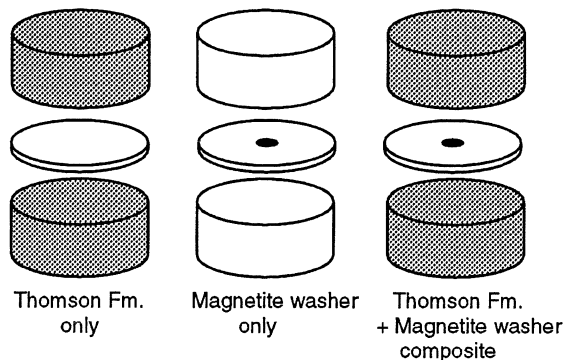


**Figure 7.** Diagram of cut Thomson Formation And nylon core samples that were then measured with either a nylon spacer or a magnetite washer inserted.

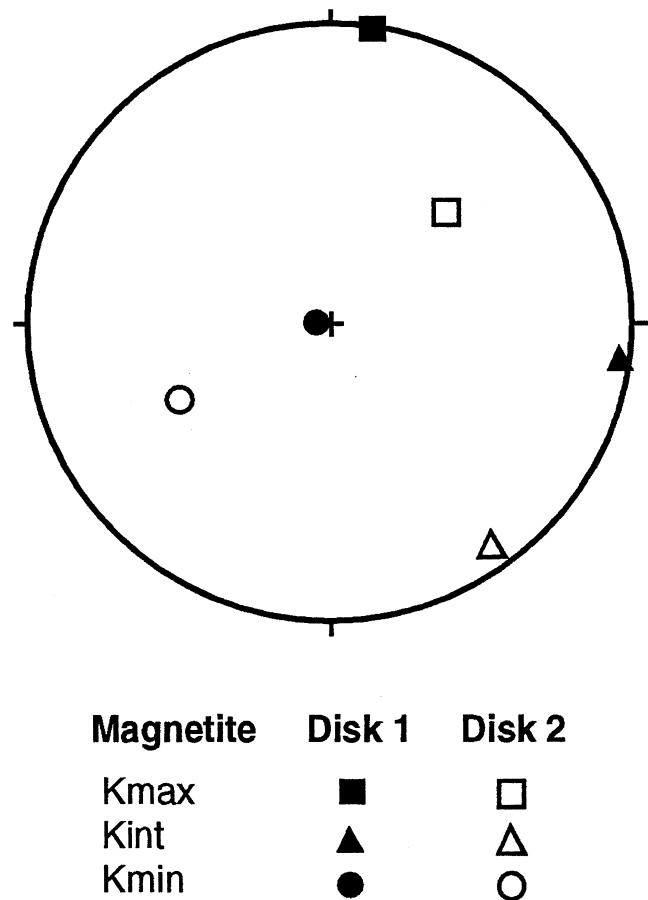


**Figure 8.** Low field AMS stereonet for magnetite discs 1 and 2 placed in the center of a split nylon cylinder.

To produce a ferromagnetic sample, we used magnetite grains from Wards Scientific Inc. (Wards sample number 46E4845 from Ishpeming, MI). This magnetite has a Curie temperature of 580° and is a very pure magnetite based on Mössbauer analysis (Peter Solheid, personal communication, 2000). These magnetite grains were glued in a 5 mm hole in the centre of a ~2 mm thick by 25 mm diameter nylon washer, which was then placed in the centre of a split 25 mm diameter diamagnetic nylon core (Fig. 7). Consequently, the entire sample was the same size as the Thomson Formation samples, but the magnetic signal was dominated by the magnetite grains at its centre. The LFAMS of this sample was measured on the KLY-2 Kappa Bridge to determine the susceptibility and fabric of the magnetite disc. Two different magnetite discs were created with different AMS principal axis orientations (Fig. 8). The two magnetite discs had bulk susceptibilities similar to those of the Thomson Formation samples (Table 1). Hysteresis loops on the two magnetite discs show that they reached saturation by 300 mT (Fig. 9). Thus, the high field slopes (~400 to 500 mT) used to calculate the HFAMS are the result of the paramagnetic minerals only.

The combination of ferromagnetic and paramagnetic behaviour was achieved by inserting the magnetite-containing nylon discs within the cut samples of the Thomson Formation. The AMS of the Thomson Formation samples was measured at both low and high field with and without the magnetite discs. LFAMS measurements run before and after HFAMS were indistinguishable from each other for all Thomson Formation samples. HFAMS was measured on the samples by the method described above.

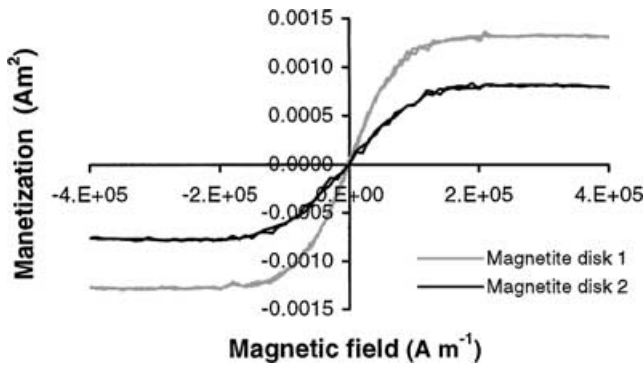


Figure 9. Hysteresis loops for magnetite disc 1 and magnetite disc 2.

RESULTS

Retrieving the paramagnetic signal

The first goal was to ascertain that the high field measurements accurately measured the paramagnetic anisotropy of the sample. The room temperature susceptibility of the Thomson Formation samples is dominated by paramagnetic minerals (clinoclore and chamosite). Consequently, the same minerals should dominate at both high and low fields. Thus, it was only necessary to compare the low field and high field measurements from the Thomson Formation, without the magnetite disc, to evaluate the accuracy of the HFAMS measurements and determine if the software was working properly. Fig. 10 shows a comparison of the low field and high field AMS where the  $K_{min}$  of the LFAMS is rotated to vertical and  $K_{max}$  is rotated to horizontal and north. The HFAMS for individual samples is rotated along with the LFAMS for comparison of the high field and low field principal directions. In general, there is good agreement between the principal directions at both high and low field (Fig. 10). The core shape is similar for all samples. Therefore, variations in the directions of  $K_{int}$  and  $K_{max}$  for samples C1, D1 and site 11 (Fig. 10a) are likely due to the samples being poorly lineated (<2 per cent). All three principal directions group well for site 13 (Fig. 10b) for which the AMS ellipsoid is distinctly triaxial, but there is a small offset between the low field and high field AMS. This effect is attributed to a natural, ferromagnetic contribution to the LFAMS that is small, but has a consistent orientation that is different from the HFAMS. For site 13, ferromagnetic minerals may account for as much as 8 per cent of the total susceptibility.

The above procedure allows us to evaluate the error in our current technique. The low field and high field AMS ellipsoids are generally oblate with  $F = K_{int}/K_{min} = 1.1-1.2$  and  $L = K_{max}/K_{int} < 1.05$  and have similar ratios for individual samples (Fig. 11). The  $K_{max}$  and  $K_{int}$  are within 5 per cent and the LFAMS and HFAMS have similar orientations for site 13 (Fig. 10b) while they are within 2 per cent for samples C1, D1 and site 11 but they show more variation between low and high field analysis (Fig. 10a). This suggests that the resolution of this HFAMS technique is <5 per cent, and probably closer to 2 per cent.

The next goal was to retrieve the paramagnetic signal in the presence of a dominant ferromagnetic signal. For the composite Thomson Formation samples with magnetite discs, the orientations of the principal low field susceptibility axes are similar to those of the magnetite-only samples (compare Figs 8 and 12). Fig. 8 shows that the low field anisotropy of the composite samples is dominated by the magnetite even though the mean susceptibility of the

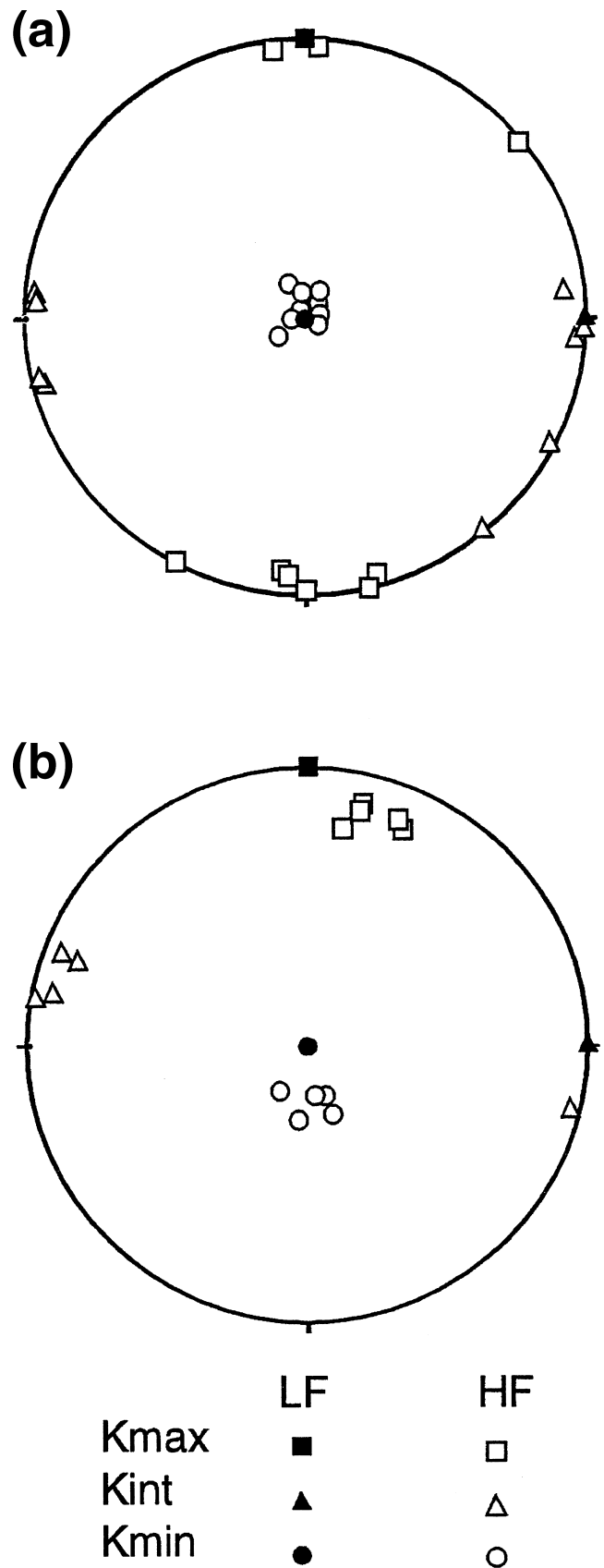
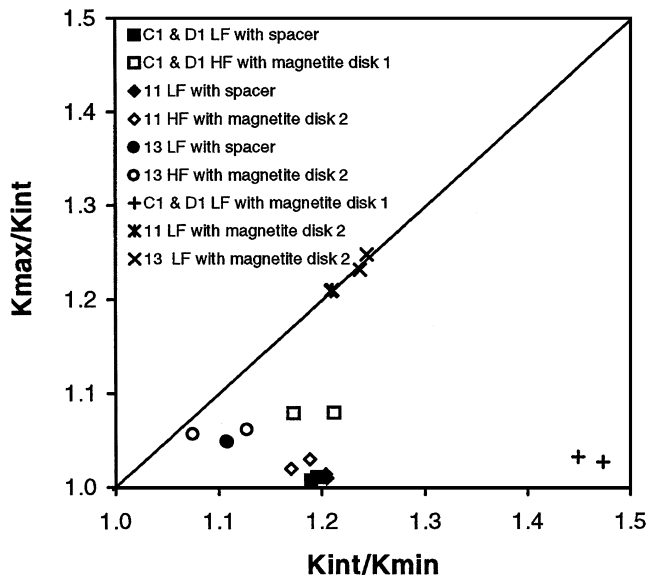


Figure 10. Comparison of high field and low field AMS for all Thomson Formation samples from (a) sites 11 and C-D; (b) site 13.



**Figure 11.** Flinn type plot of high field and low field AMS data for the split Thomson Formation cores showing that the HFAMS fabric of Thomson Formation plus magnetite washer (open symbols) is similar to the LFAMS for the Thomson Formation with nylon disc (closed symbols) and both are very different from the LFAMS for these samples with the magnetite washer (+, \* and x).

paramagnetic Thomson Formation and the magnetite disc are similar. However, the HFAMS directions for the composite samples are similar to those of the unmodified Thomson Formation samples (Fig. 12). This observation demonstrates that the HFAMS is dominated by the paramagnetic minerals and that there is little contribution from the magnetite disc. We interpret this result to imply that the peak fields used were sufficient to saturate the ferromagnetic contribution of the magnetite disc.

The LFAMS with the nylon spacer and the HFAMS with the magnetite disc have similar principal directions for each sample (Fig. 13). This result shows that the HFAMS successfully isolates the paramagnetic component of AMS. The difference between low and high field Kint and Kmax in Fig. 13(b) is a result of the highly

oblate AMS in this sample. The difference between high and low field directions in Figs 13(e) and (f) is likely due to a small natural ferrimagnetic contribution to the LFAMS of site 13 samples, as in Fig. 10(b). The magnitudes of the foliation and lineation are also similar for these measurements (Fig. 11). This is consistent with the original sample's LFAMS being dominated by paramagnetic minerals. Both the low and high field results are reproducible as can be seen from the data for samples 13.3b and C1, Figs 12(b) and 13(a) respectively. Thus, the HFAMS has successfully removed the ferromagnetic contribution of the magnetite disc.

*Calculation of the ferromagnetic signal*

Our method also allows calculation of the ferromagnetic AMS signal. The low field susceptibility for the Thomson Formation with a magnetite disc is the result of the ferromagnetic plus paramagnetic contributions. The high field measurement on the same sample measures only the paramagnetic signal. Consequently, the ferromagnetic AMS can be calculated via subtraction of the HFAMS from the LFAMS. As both the high field and low field AMS are second order tensors (e.g. Tarling & Hrouda 1993), the operation involves tensor subtraction (Appendix B). Since the ferromagnetic AMS is due to the magnetite disc, this data is directly comparable with the magnetite disc measured within the nylon core.

These calculations were completed for the six split samples of the Thomson Formation measured while they contained a magnetite disc. Fig. 14 shows a very good correlation between the ferromagnetic AMS calculated by the subtraction of the high field from the low field AMS and the AMS of the magnetite disc measured at low field while centred in the nylon core. Thus, the ferromagnetic susceptibility also is accurately determined with this method.

**DISCUSSION**

*Potential application of technique*

We have shown that these high field anisotropy measurements separate the ferromagnetic and paramagnetic AMS components, using standard palaeomagnetic cores. Our experimental approach used

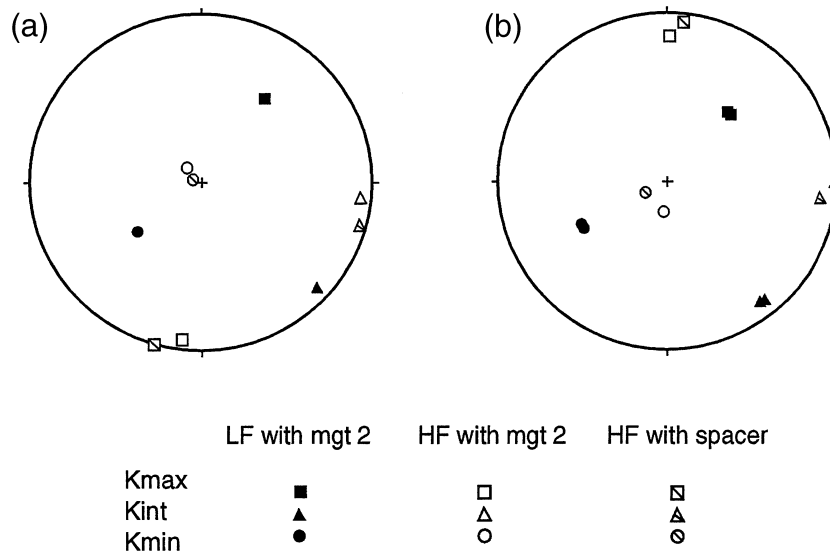


**Figure 12.** Principal AMS axes plotted for the Thomson Formation plus magnetite at both low field and high field, and Thomson Fm plus spacer at high field for: (a) sample 11.2 and (b) sample 13.3b.

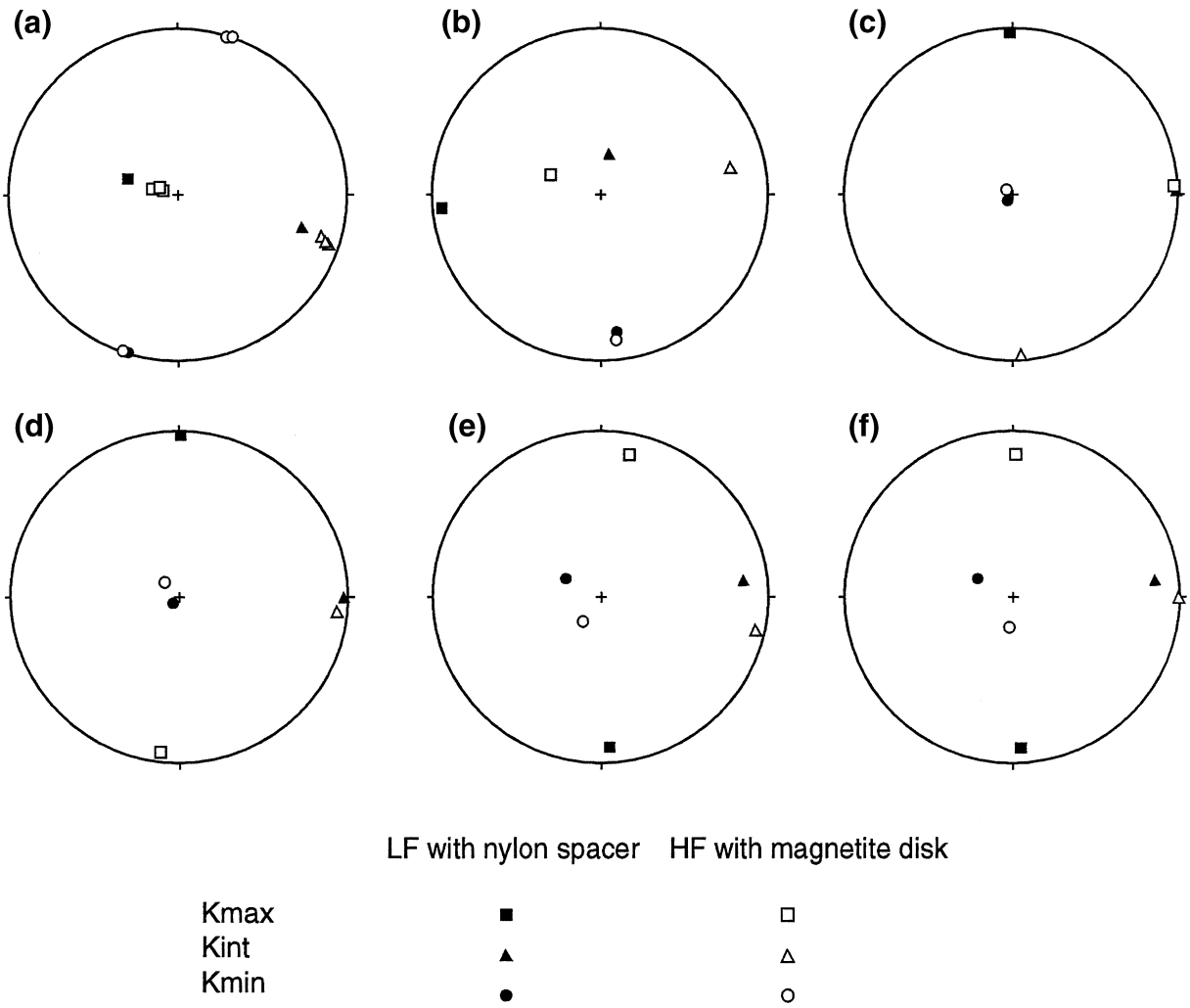


**Figure 13.** Stereonets of principal AMS directions for split Thomson Formation Cores with nylon spacer at low field and magnetite disk at high field for samples: (a) C1, (b) D1, (c) 11.1a, (d) 11.2, (e) 13.3a, (f) 13.3b. The low susceptibility is the natural primarily paramagnetic, AMS. The HFAMS is also primarily due to the paramagnetic minerals since the susceptibility is measured at fields greater than necessary to saturate the magnetite component.

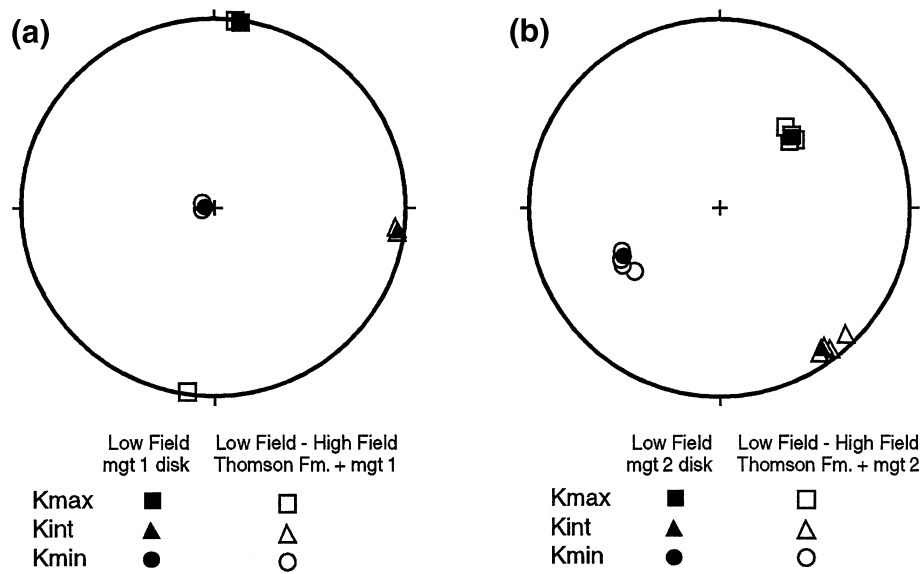


**Figure 14.** Ferromagnetic AMS from the magnetite discs measured in the nylon cylinder compared to the ferromagnetic AMS determined by the subtraction of the HFAMS from the LFAMS for (a) magnetite disc 1; (b) magnetite disc 2.

cores from the Thomson Formation, which are dominantly paramagnetic, combined with magnetite grains of a known AMS signal. The advantage of this approach is that we knew, *a priori*, the AMS of the individual components, and could directly verify that the high field method separated the paramagnetic AMS signal. By tensor subtraction, the orientation and magnitude of the ferromagnetic AMS was also retrieved and confirmed with independent measurements of the ferromagnetic AMS. Although these samples were natural, they were artificially combined to test the method. However, we believe that this technique has applications for a wide variety of geological situations.

Naturally deformed rocks typically have different sub-populations of mineral grains. Workers interested in fabric analyses in granites have noted these different orientations, as a result of order of crystallization, deformation, or late-stage sub-magmatic fracturing (Borradaile & Henry (1997); Bouchez *et al.* (1992)). Using simultaneous low-field and high-field measurements is a relatively rapid way of separately determining the fabrics for the paramagnetic and the ferromagnetic components of the rock. Consequently, one can potentially determine the fabrics associated with different deformation phases, provided that different minerals are involved.

Another possible application for this technique is to rocks with secondary magnetite. For example, ultramafic rocks often contain abundant secondary magnetite as the result of olivine altering to serpentine plus magnetite. This secondary magnetite typically dominates the LFAMS, whose geological significance is therefore unclear. Removing the ferromagnetic signal allows determination of the AMS of the paramagnetic silicates, which is potentially related to magmatic or solid state flow structures and thus has more direct petrologic and tectonic significance.

In addition, this technique can help in the case where the results of the ferromagnetic minerals provide a confusing signal. Both single-domain and multi-domain magnetite contribute to the AMS signal, although the former results in an inverse fabric (Potter & Stephenson 1988). Consequently, in rocks with a significant portion of both single-domain and multi-domain magnetite, the paramagnetic mineral will likely provide a more direct relationship to rock fabric.

This technique is applicable for ferromagnetic minerals that saturate at fields below 500 mT for our current methodology. Some natural materials, including antiferromagnetic minerals such as hematite, goethite and pyrrhotite, require much larger fields to achieve saturation. The magnetization of these materials will also contribute to the HFAMS, and thus, in this situation, HFAMS should not be interpreted as a simply the result of paramagnetic minerals. Care must be taken to assure that ferromagnetic saturation has been achieved before interpretation of high field and low field AMS.

#### *Methods for improving technique*

A variety of adaptations to the method described above might be undertaken to potentially increase accuracy or decrease measurement time. The use of cubic samples instead of cores would allow the shape effect to be mathematically subtracted without the use of an isotropic standard of the same shape as the samples (Ferre *et al.* 2000; Thill *et al.* 2000). A perfectly-centred homogeneous isotropic cube exhibits a pure  $\sin(4\theta)$  variation due to shape when the sample is rotated around any face centred axis. Thus, the shape effect can be removed by using a Fourier filter which eliminates the  $4\theta$  term (e.g. Rochette & Fillion 1988), and more importantly, no  $\sin(2\theta)$  correction is necessary.

The maximum field used in our experiments ( $\sim 500$  mT) is just sufficient to saturate most single-domain magnetites, as these grains typically have a higher coercivity than multiple domain magnetites. Other ferromagnetic minerals may also require higher saturating fields. Consequently, methods that allow larger applied fields by decreasing pole separation will return more robust results. The use of samples smaller than the standard  $10\text{ cm}^3$  cores used in this study would allow closer pole spacing, and would allow larger fields to be generated. However, caution is required, because sample shape effects are much stronger with narrow spacings, and because smaller samples may not be representative of the bulk mass.

Measurement times can be reduced significantly if measurements are made only for the high field part of a hysteresis loop that is used to calculate the paramagnetic susceptibility, instead of measuring the entire loop. Significant reduction in measurements time is also possible if measurements are made for fewer orientations as is typical in most LFAMS studies (e.g. 7–15, Borradaile & Stupavsky 1995), compared to our 24 orientations. The above modifications would likely result in reduction in measurement time by one half or more. However, fewer orientations could introduce additional errors as discussed in Appendix C. High field hysteresis loops were measured in 24 different orientations in this study.

Since complete hysteresis loops were collected in all orientations, information related to the ferromagnetic character of the sample is collected also. This data includes saturation remanent magnetization and coercivity. Since this data is collected in each orientation as part of the standard hysteresis loops, its anisotropy could be analysed. Thus, information about the magnitude and type of anisotropy for both the paramagnetic and ferromagnetic minerals can be examined from these hysteresis loops. Additionally, if the ferromagnetic material is uniformly distributed through the sample, the measured directional values of saturation magnetization can be used to obtain an independent estimate of sample shape and miscentring effects.

## SUMMARY AND CONCLUSIONS

Our experiments demonstrate the separation of the paramagnetic and ferromagnetic AMS contributions for samples containing a significant component of both ferromagnetic and paramagnetic susceptibility. Our technique was to apply high magnetic fields, which saturate the ferromagnetic minerals, and use the high field slope (the change in induced magnetization for changes in applied field at high field values) to calculate the paramagnetic directional susceptibilities. We were able to successfully saturate the ferromagnetic component and to correct for significant shape effects in these high field measurements. Natural samples of dominantly paramagnetic material (Thomson Formation) and ferromagnetic material (magnetite) were measured separately and then physically combined and measured again. Using the high field slope, one can eliminate the ferromagnetic component and determine the magnetic fabric resulting solely from the paramagnetic component which is often more directly related to rock forming processes than then ferromagnetic fabric. Using this information, in combination with LFAMS measurements which are the result of the paramagnetic plus ferromagnetic susceptibility, it is also possible to calculate the magnetic fabric resulting solely from the ferromagnetic component. This new method promises to be useful in the interpretation of AMS from rocks with a significant susceptibility from both paramagnetic and ferromagnetic minerals. As currently described this technique can resolve anisotropies of  $>2$  per cent and thus caution should be exercised if

samples have weak anisotropies or a heterogeneous distribution of magnetic minerals.

## ACKNOWLEDGMENTS

Funding for this project was provided by the David and Lucille Packard Foundation to BT and an Institute for Rock Magnetism (University of Minnesota) visiting fellowship to PK and BT. John Marchetti and coworkers at the engineering shop at the University of Minnesota fabricated sample holders for the high field VSM measurements. Many thanks are due to them for building multiple versions of the equipment in the pursuit of a suitable design. Significant improvements to the equipment design were suggested by Christian Teyssier. PK and BT wish to thank the entire IRM group for their hospitality during our visit. We thank Eric Ferre, Pierre Rochette, Franstisek Hrouda for constructive comments on previous versions of this manuscript, Jim Marvin and Jim Thill for helpful discussions concerning high-field anisotropy measurements, and Sarah Titus for assistance in the lab. The Institute for Rock Magnetism is supported by a grant from the Instruments and Facilities Programme, Earth Science Division, the National Science Foundation. This is IRM contribution number 01–03.

## REFERENCES

- Aubourg, C., Rochette, P. & Bergmüller, F., 1995. Composite magnetic fabric in weakly deformed black shales, *Phys. Earth planet. Int.*, **87**, 267–278.
- Bailey, S.W., 1988. Chlorites: structure and crystal chemistry, in *Hydrous Phyllosilicates (exclusive of micas)*, Vol. 19, pp. 347–401, ed. Bailey, S.W., Rev. Mineral., Mineral. Soc. Am., Washington, D.C.
- Banerjee, S.K. & Stacey, F.D., 1967. The high-field torque-meter method of measuring magnetic anisotropy in rocks, in *Methods in Palaeomagnetism*, pp. 470–476, eds. Collinson, D.W., Creer, K.M. & Runcorn, S.K., Elsevier, Amsterdam.
- Bergmüller, F. & Heller, H., 1996. The field dependence of magnetic anisotropy parameters derived from high-field torque measurements, *Phys. Earth planet. Int.*, **96**, 61–76.
- Borradaile, G.J. & Stupavsky, M., 1995. Anisotropy of magnetic susceptibility: measurements schemes, *Geophys. Res. Lett.*, **15**, 1957–1960.
- Borradaile, G.J., & Henry, B., 1997. Tectonic applications of magnetic susceptibility and its anisotropy, *Earth Sci. Rev.*, **42**, 49–93.
- Borradaile, G.J., & Keeler, W., Alford, C. & Sarvas, P., 1987. Anisotropy of magnetic susceptibility of some metamorphic minerals, *Phys. Earth planet. Int.*, **48**, 161–166.
- Bouchez, J.L., Delas, C., Gleizes, G., Nedelec, A. & Cuney, M., 1992. Submagmatic microfractures in granites, *Geology*, **20**, 35–38.
- Collinson, D.W., 1983. *Methods in Rock Magnetism and Palaeomagnetism*, Chapman and Hall, London.
- Collombat, H., Rochette, P. & Kent, D.V., 1993. Detection and correction of inclination shallowing in deep-sea sediments using the anisotropy of anhysteretic remanence, *Bull. Soc. Géol. France*, **164**, 103–111.
- Deer, W.A., Howie, R.A. & Sussman, J., 1966. *An Introduction to the Rock-Forming Minerals*, Wiley, New York.
- Dunlop, D.J. & Özdemir, Ö., 1997. *Rock Magnetism: Fundamental and Frontiers*, Cambridge University Press, Cambridge, UK.
- Ferre, E.C., Thill, J.W., Rainey, E.S.G. & Teyssier, C., 2000. Ductile flow in migmatites deduced from combined low- and high-field AMS measurements, *EOS, Trans. Am. geophys. Un.*, **81**, 366.
- Folami, S.L. & Hailwood, E.A., 1991. Magnetic Fabric Results from DSDP Holes 380A (Black Sea) and 524 (South Atlantic) sediment cores: A case study of the comparison between low and high field torque magnetometer measurements, *Mar. Geophys. Res.*, **13**, 239–253.
- Graham, J.W., 1954. Magnetic susceptibility anisotropy, an unexploited petrofabric element, *Geol. Soc. Am. Bull.*, **65**, 1257–1258.
- Girdler, R.W., 1961. The measurement and computation of anisotropy of magnetic susceptibility in rocks, *Geophys. J. R. astr. Soc.*, **5**, 34–44.
- Henry, B., 1985. Magnetic fabrics and superimposed deformations: example of Dalradian rocks from the southwest Highlands of Scotland, *Phys. Earth planet. Int.*, **40**, 187–200.
- Henry, B. & Daly, L., 1983. From qualitative to quantitative magnetic anisotropy analysis: the prospect of finite strain calibration, *Tectonophysics*, **98**, 327–336.
- Holst, T.B., 1984. Evidence for nappe development during the early Proterozoic Penokean orogeny, Minnesota, *Geology*, **12**, 135–138.
- Hrouda, F., 1987. Mathematical model relationship between the paramagnetic anisotropy and strain in slates, *Tectonophysics*, **142**, 323–327.
- Hrouda, F., 1994. A technique for the measurement of thermal changes of magnetic susceptibility of weakly magnetic rocks by the CS-2 apparatus and KLY-2 Kappabridge, *Geophys. J. Int.*, **118**, 604–612.
- Hrouda, F., 2002. The use of the anisotropy of magnetic remanence in the resolution of the anisotropy of magnetic susceptibility into its ferromagnetic and paramagnetic components, *Tectonophysics*, **347**, 269–281.
- Hrouda, F. & Jelínek, V., 1990. Resolution of ferrimagnetic and paramagnetic anisotropies in rocks, using combined low-field and high-field measurements, *Geophys. J. Int.*, **103**, 75–84.
- Hrouda, F., Jelínek, V. & Zapletal, K., 1997. Refined technique for susceptibility resolution into ferromagnetic and paramagnetic components based on susceptibility temperature-variation measurement, *Geophys. J. Int.*, **129**, 715–719.
- Ising, G., 1943. On the magnetic properties of varved clay: I, Line of investigation; measurements on a varve series from Viby in southern Sweden, *Arkiv Mat. Astron. och Fysik*, **29 A**, 1–37.
- Jackson, M.J., 1991. Anisotropy of magnetic remanence: a brief review of mineralogical sources, physical origins, and geological applications, and comparison with susceptibility anisotropy, *Pageoph*, **136**, 1–28.
- Jackson, M.J. & Tauxe, L., 1991. Anisotropy of magnetic susceptibility and remanence: developments in the characterization of tectonic, sedimentary, and igneous fabric, *Rev. Geophys.*, **29**, suppl. (IUGG Report–Contrib. Geomagn. Paleomagn. 1987–1990), 371–376.
- Jelínek, V., 1973. Precision A.C. bridge set for measuring magnetic susceptibility of rocks and its application, *Stud. Geophys. Geod.*, **17**, 36–48.
- Johns, M.K., Jackson, M.J. & Hudleston, P.J., 1992. Compositional control of magnetic anisotropy in the Thomson formation, east-central Minnesota, *Tectonophysics*, **210**, 45–58.
- Kadzialko-Hofmök, M., 1986. High-field magnetic anisotropy of oriented samples of lower Silesian basaltic rocks, *Acta Geophys. Polonica*, **34**, 361–375.
- Martín-Hernández, F. & Hirt, A.M., 2001. Separation of ferrimagnetic and paramagnetic anisotropies using a high-field torsion magnetometer, *Tectonophysics*, **337**, 209–221.
- McCabe, C., Jackson, M.J. & Ellwood, B.B., 1985. Magnetic anisotropy in the Trenton limestone: results of a new technique, anisotropy of anhysteretic susceptibility, *Geophys. Res. Lett.*, **12**, 333–336.
- Morey, G.B., 1983a. Lower Proterozoic stratified rocks and the Penokean Orogeny in east-central Minnesota, in *Early Proterozoic Geology of the Lake Superior Region*, Vol. 160, pp. 97–122, ed. Medaris, L.J. Jr., Mem. Geol. Soc. Am.
- Moskowitz, B.M., Jackson, M.J. & Kissel, C., 1997. Low-temperature magnetic behavior of titanomagnetites, *Earth planet. Sci. Lett.*, **157**, 141–149.
- Owens, W.H. & Bamford, D., 1976. Magnetic, seismic, and other anisotropic properties of rock fabrics, *Phil. Trans. R. Soc. Lond., A.*, **283**, 55–68.
- Parma, J., 1988. An automated torque meter for rapid measurement of high-field magnetic anisotropy of rocks, *Phys. Earth planet. Int.*, **51**, 387–389.
- Potter, D.K. & Stephenson, A., 1988. Single-domain particles in rocks and magnetic fabric analysis, *Geophys. Res. Lett.*, **15**, 1097–1100.
- Richter, C. & van der Pluijm, B.A., 1994. Separation of paramagnetic and ferrimagnetic susceptibilities using low temperature magnetic susceptibilities and comparison with high field methods, *Phys. Earth planet. Int.*, **82**, 111–121.
- Rochette, P., 1994. Comments on ‘Magnetic Fabric, Crystallographic, Preferred Orientation, and Strain of Progressively Deformed Metamorphosed

*Pelites in the Helvetic Aone of the Central Alps (Quartenschiefer Formation)*, eds Richter, C., Ratschbacher, L. & Frisch, W., *J. geophys. Res.*, **99**, 21 825–21 827.

Rochette, P. & Fillion, G., 1988. Identification of multicomponent anisotropies in rocks using various field and temperature values in a cryogenic magnetometer, *Phys. Earth planet. Int.*, **51**, 379–386.

Rochette, P., Jackson, M.J. & Aubourg, C., 1992. Rock magnetism and the interpretation of anisotropy of magnetic susceptibility, *Rev. Geophys.*, **30**, 209–226.

Sims, P.K., Van Schmus, W.R., Schultz, K.J. & Peterman, Z.E., 1989. Tectono-stratigraphic evolution of the Early Proterozoic Wisconsin magmatic terranes of the Penokean Orogen, *Can. J. Earth Sci.*, **26**, 2145–2158.

Southwick, D.L., Morey, G.B. & McSwiggen, P.L., 1988. Geologic map of the Penokean Orogen, central and eastern Minnesota and accompanying text, *Minn. Geol. Surv. Rep. Invest.*, **37**.

Sun, W.-W., Hudleston, P.J. & Jackson, M.J., 1995. Magnetic and petrofabric studies in the multiply deformed Thomson Formation, east-central Minnesota, *Tectonophysics*, **249**, 109–124.

Tarling, D.H. & Hrouda, F., 1993. *The Magnetic Anisotropy of Rocks*, Chapman and Hall, London.

Thill, J.W., Ferre, E.C., Rainey E.S.G. & Teyssier, C., 2000. Separation of AMS into ferrimagnetic and paramagnetic components in migmatites: A possible shear-sense indicator?, *EOS, Trans. Am. geophys. Un.*, **81**, 367.

Van Schmus, W.R., 1976. Early and Middle Proterozoic history of the Great Lake area, North America, *Phil. Trans. R. Soc. Lond., A.*, **280**, 605–628.

Van Schmus, W.R., 1980. Chronology of igneous rocks associated with the Penokean orogeny in Wisconsin, *Geol. Soc. Am. Spec. Paper*, **182**, 159–168.

## APPENDIX A: VSM SIGNAL RESPONSE EFFECTS

A VSM measures the voltage induced in a set of pickup coils by the time-varying magnetic flux due to the vibration of the sample. Various pick-up coil geometries can be used; in ours (Princeton Measurements Corp model 3900) two oppositely-wound coplanar circular coils are mounted, one above the other, on each magnet pole face, as shown in Figs 4 and A1. We define a coordinate system whose origin is centred between the four coils, with the  $y$ -axis parallel to the field and perpendicular to the coil planes, and the  $z$ -axis vertical. A point magnetic dipole of moment  $\mathbf{m}$ , located at a point  $P$  in the measurement region, produces a  $\mathbf{B}$  field whose radial and tangential components at a point  $P'$  in one of the pickup coils are:

$$B_r = \frac{\mu_0 m}{4\pi} \times \frac{2 \cos(\theta)}{r^3}$$

and

$$B_\theta = \frac{\mu_0 m}{4\pi} \times \frac{\sin(\theta)}{r^3}$$

The component normal to the coil is:

$$B_y = B_r \cos(\theta) - B_\theta \sin(\theta) = \frac{\mu_0 m}{4\pi r^3} \times (2 \cos^2(\theta) - \sin^2(\theta))$$

Defining the components of the vector  $\mathbf{r}$  as  $u = x' - x$ ,  $v = y' - y$ , and  $w = z' - z$ , we can rewrite  $B_y$  as:

$$B_y = \frac{\mu_0 m}{4\pi} (2v^2 - u^2 - w^2)(u^2 + v^2 + w^2)^{-5/2}$$

As the sample vibrates vertically according to  $z(t) = z_0 + A \sin(\omega t)$ , the field at  $P'$  varies as:

$$\frac{\partial B_y}{\partial t} = \frac{\partial B_y}{\partial z} \frac{dz}{dt} = \frac{\partial B_y}{\partial w} \frac{dz}{dt} = \frac{\mu_0 m \omega A}{4\pi} 2w(u^2 + v^2 + w^2)^{-5/2} \left[ \frac{(-5/2)(2v^2 - u^2 - w^2)}{(v^2 + u^2 + w^2)} - 1 \right]$$

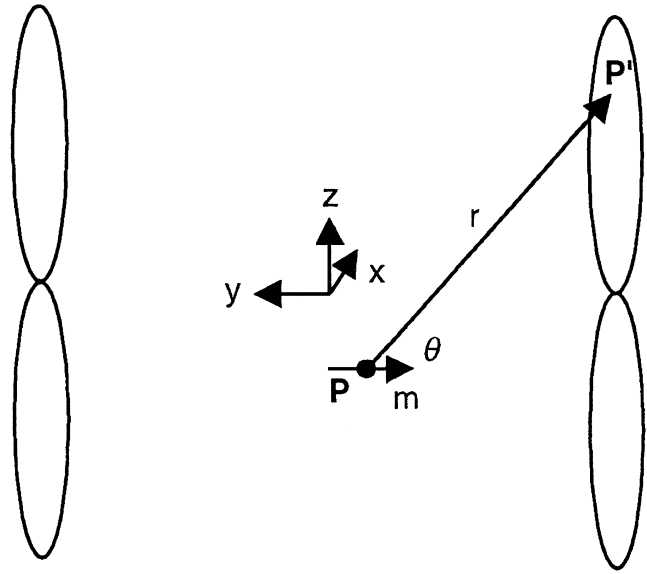


**Figure A1.** A perspective diagram of the geometry used to model VSM response function. The infinitesimal dipole sample at point  $P$  has moment  $\mathbf{m}$ , oriented along the applied field axis in the  $y$  direction. Circular pickup coils are oriented perpendicular to the field axis (in the  $x$ - $z$  plane). The  $y$ -component of the field due to  $\mathbf{m}$  at a point  $P'$  varies with time as the sample vibrates vertically.

The voltage in each pickup coil is calculated by integrating  $\delta B_y / \delta t$  over the area ( $a$ ) of the coil:

$$V = \oint_{\text{coil}} \bar{\mathbf{E}} \cdot d\bar{s} = \int_{\text{area}} (\bar{\nabla} \times \bar{\mathbf{E}}) \cdot d\bar{a} = \int_{\text{area}} \frac{\partial B_y}{\partial t} d\bar{a}$$

Where  $\mathbf{E}$  is the electric field and  $s$  is around the length of the coil. Numerical integration and summing the voltages for the four coils yields the signal strength for a magnetic dipole at any point  $P$  in the measurement space. Fig. A2 compares the calculated and measured signals for a small piece of Ni foil at various positions along the  $y$ -axis, and shows that the calculations accurately describe the system behaviour. For narrow pole gaps (less than the diameter of the pickup coils), the response is relatively flat. With larger pole gaps, the system becomes increasingly sensitive to relative displacements in the  $y$  direction. At a point midway between the origin and the coil plane (relative displacement = 0.5), the measured moment may be three or more times the true value, if the pole gap is several times the coil diameter.

Now let's consider how the VSM response is affected by sample shape. A spherical sample, properly centred, occupies precisely the same volume in any measurement orientation. For any other specimen shape, different parts of the measurement space are occupied in different orientations, and the measured moment, which integrates the VSM response function over the sample volume, varies accordingly.

We have evaluated the magnitude of geometric effects by numerically integrating the VSM response function over a variety of isotropic, homogeneous samples. We focus on cylindrical specimens because they are widely used, due to the convenience of sampling by rotary coring. A typical sample set contains cylinders of relatively uniform diameter and somewhat more variable lengths (typically 0.8–0.9 times the diameter). A cylinder rotated about one of its equatorial axes will periodically occupy different regions of higher and lower sensitivity. The difference between axial and equatorial

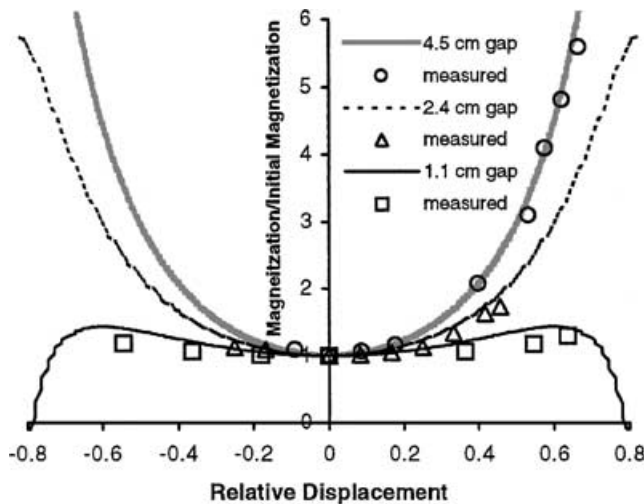


**Figure A2.** Comparison of model (curves) and measured (points) variations in signal strength for a point dipole with displacement in the  $y$  direction (along the field axis) for pole gaps of 11, 24 and 45 mm.

aspects generates a shape-effect signal that varies as a function of  $\sin(2\theta)$ . Additionally, the corners of the sample pass in turn through the high-sensitivity region near the pickup coils, generating four maxima per rotation, a  $\sin(4\theta)$  variation. The  $\sin(4\theta)$  variation can not be confused for an anisotropy signal, whereas a  $\sin(2\theta)$  variation can. Consequently, although both variations are of comparable amplitude, the  $\sin(2\theta)$  variation is more consequential.

Correcting for the sample shape effect is accomplished by normalizing each measured magnetic moment by the integrated response function over the sample in the corresponding orientation and position. The response function integrals are obtained either: (1) theoretically, as in these models, or (2) empirically, by measurement of homogeneous isotropic standard samples of the appropriate size and shape, in the same set of orientations. We used an empirical approach (Fig. 6).

Finally, we evaluated the potential effects of heterogeneity. Consider a sample that is composed of discrete volume elements, which are identical except for one which is significantly more magnetic. As the sample is rotated into different orientations in the measurement space, each volume element (including the anomalous one) follows a circular orbit around the rotation axis and moves through regions of high and low instrument sensitivity. The resulting angular variation in measured moments would be the sum of the signal generated by a homogeneous sample of the same shape, and the signal due to the orbiting anomaly. The latter would be dominated by a  $2\theta$  variation, with maxima when the anomaly passed by either set of coils, and minima when it was in the lower-sensitivity regions at right angles to the field axis.

In principle it is possible to determine the distribution of magnetization in a heterogeneous sample by 3-D deconvolution. In practice, however, the large number of additional measurements required, and the necessary displacement precision, make such an approach impractical. Consequently, heterogeneity is a residual source of error. For additional discussions and calculations of potential errors see Appendix C.

## APPENDIX B: DATA PROCESSING

A series of three computer programs were used to analyse the HFAMS data from each sample. The purpose of the first programme

(written by J. Marvin and modified by B. Tikoff and J. Marvin) was to calculate the high-field slope from the VSM data. This calculation was achieved by calculating an average slope for the highest applied field values (top 8 per cent). The measurements at the highest applied field were omitted, as they were prone to slight measurement errors which artificially lowered the slope of the line. For any individual hysteresis loop, the four high-field slope measurements were averaged into a single value (i.e. moving away from high positive values, moving toward high negative values, moving away from high negative values, moving toward high positive values).

The purposes of the second programme (written by M. Jackson, modified by B. Tikoff and M. Jackson) are to: (1) average measurements along the same orientations for consistency; (2) normalize out the shape effect; (3) normalize the  $X$ ,  $Y$  and  $Z$  axis rotations with respect to each other; and (4) output the data in a format acceptable for calculation of the eigenvalues and eigenvectors using the same software used for the LFAMS calculations. For the eight  $45^\circ$  rotation steps around each axis, the positions oriented  $180^\circ$  from each other should have identical values (positive and negative). Consequently, for each rotation, there were four independent measurements. The removal of the shape effect was based on normalizing each directional measurement by the corresponding measurement for the  $\text{MnO}_2$  standard. Because of the isotropic and paramagnetic nature of the standard, any variation of the signal for the  $\text{MnO}_2$  was interpreted to result from the response-function shape effect. This was confirmed by LFAMS measurements on the KLY2 which show an anisotropy for the  $\text{MnO}_2$  of less than 0.3 percent. Normalization, in essence, divides each measured value by the response function integral for a sample of the standard size and shape in the appropriate orientation. This approach should work for any amount of anisotropy, provided that there is not a strong heterogeneity, i.e. not all of the highly magnetic materials are located on the edges of the sample.

This second programme then adjusts for inconsistencies between the rotations ( $X$ ,  $Y$  and  $Z$ ) which result from inexact vertical centring after removal and reinsertion of the sample between rotations. This normalization is accomplished by noting that each rotation shares one position with another rotation. In other words, the  $X$  and  $Y$ -axis rotations both measure the same position (along the  $Z$  axis) once, and likewise with the  $X$  and  $Z$  rotations and the  $Y$  and  $Z$  rotations. Consequently, there are really only 9 independent measurements, rather than 12, for each sample. Both the  $X$  and  $Y$  loops are normalized to match the intersecting  $Z$  loop values, because the  $Z$  loop has a negligible shape correction. A normalization factor is calculated between the  $X$  and  $Z$  loops using the shared orientation measurement, and all the  $X$  values are multiplied by this factor. The same process is repeated for the  $Y$  orientations.

The magnitude and direction of the AMS ellipsoid is then calculated by entering the high field susceptibility values into the programme that operates the KLY-2 Kappa bridge at the IRM at the University of Minnesota (modified from the original vendor software by T. Torsvik). This is a simple substitution because the low field and high-field measurements are made in same orientations.

The high-field susceptibility tensor obtained by the procedures above represents the AMS of dia-, para- and antiferromagnetic material in the sample. The LFAMS measured on the Kappa bridge, includes these contributions along with those of the ferromagnetic grains. The ferromagnetic susceptibility tensor can therefore be obtained by subtraction of the HFAMS tensor from the LFAMS tensor, element by element. A fourth programme (written by M. Jackson) calculates the ferromagnetic AMS by tensor subtraction, and computes its eigenvalues and eigenvectors.

The above programs (and associated hardware) exist at the Institute for Rock Magnetism at the University of Minnesota and are available for use by future visiting fellows to the Institute.

### APPENDIX C: ERROR ANALYSIS

The 15 orientations used in the standard Kappa-bridge AMS analysis represent a subset of the 24 orientations measured during our HFAMS. Specifically, the HFAMS procedure makes three additional measurements parallel to each of the sample coordinate axes. For convenience we have averaged together the four measured high field susceptibility values for each coordinate axis, yielding a data set with 15 directional values, for processing with the Kappa software.

Error analysis in the Kappa software uses the statistical methods of Jelínek (1973). Under the assumption that measurement errors are normally-distributed, F-tests are used to evaluate the significance of the magnetic lineation, foliation, and total anisotropy 95 per cent-confidence angles are given for the principal axis orientations.

In the analysis of high-field data, non-random errors—in addition to random measurement errors—may be significant. These include sample shape and heterogeneity, as described in Appendix A. Another possible source of systematic error is incomplete saturation of the ferromagnetic material. High field susceptibility is calculated from the hysteresis loops by determining the slope for data from the highest 8 per cent of the magnetic field. If the ferromagnetic contribution to the high-field slope is nonzero, the paramagnetic susceptibility is overestimated accordingly, i.e. high field susceptibility = paramagnetic susceptibility + high field ferromagnetic susceptibility. In the following paragraphs, we consider how these non-random errors are propagated through the calculations, and how they affect the results using standard matrix calculations (e.g. Girdler 1961; Borradaile & Stupavsky 1995).

The six independent elements of the susceptibility tensor ( $k^T$ ) can be arranged in a column matrix  $\mathbf{k}$ , where  $\mathbf{k}^T = (k_{11}, k_{22}, k_{33}, k_{12}, k_{23}, k_{31})$ . For susceptibility measurements that detect only the component of magnetization parallel to the applied field (as in standard AMS analysis using instruments like the Kappabridge, and in our HFAMS method using a VSM), the expected value for each directional measurement  $M_i$  is the scalar product of a row vector  $\mathbf{d}_i$  and  $\mathbf{k}$ , where  $\mathbf{d}_i = (\alpha_1^2, \alpha_2^2, \alpha_3^2, \alpha_1\alpha_2, 2\alpha_2\alpha_3, 2\alpha_3\alpha_1)$ . The  $\alpha$  variables are the direction cosines of the applied field direction in the sample coordinate system. The expected values for a set of directional measurements form a column matrix  $\mathbf{M}$ , where  $\mathbf{M}^T = (M_1, M_2, \dots, M_N)$ , which is the product of the  $N \times 6$  matrix  $\mathbf{D}$  (with rows  $\mathbf{d}_1, \mathbf{d}_2, \dots, \mathbf{d}_N$ ) and  $\mathbf{k}$ :  $\mathbf{M} = \mathbf{D}\mathbf{k}$ .

In practice,  $\mathbf{k}$  is unknown and is determined from directional measurements. The least-squares solution for  $\mathbf{k}$ , given a data set  $\mathbf{M}'$ , is  $\mathbf{k}' = (\mathbf{D}^T\mathbf{D})^{-1}\mathbf{D}^T\mathbf{M}'$ . For error-free data ( $\mathbf{M}' = \mathbf{M}$ ), the solution is exact ( $\mathbf{k}' = \mathbf{k}$ ). With measurement errors, the uncertainty in  $\mathbf{k}'$  is directly related to the uncertainty in  $\mathbf{M}'$ :  $\Delta\mathbf{k} = \mathbf{G}\Delta\mathbf{M}$ , where  $\mathbf{G} = (\mathbf{D}^T\mathbf{D})^{-1}\mathbf{D}^T$ . For normally-distributed, zero-mean errors,  $\mathbf{k}'$  is the unbiased maximum likelihood estimate of  $\mathbf{k}$ , and statistical estimates of  $\Delta\mathbf{M}$ , e.g. the standard errors estimated from redundant measurements, translate directly into standard errors for the  $k_i$ .

Systematic errors in the data lead to biased estimates of  $\mathbf{k}$ , but these can still be evaluated exactly according to  $\Delta\mathbf{k} = \mathbf{G}\Delta\mathbf{M}$ . Let us consider nonsaturation of ferromagnetic material, which would result in systematic overestimates of  $k_p$  as mentioned above. Suppose that the ferromagnetic contribution to the high-field slope is independent of orientation, i.e.  $\Delta M_i$  has a constant positive value for all  $i$ . It is easy to show that the resultant errors are  $\Delta k_{ij} = \delta_{ij}\Delta M$

(where the delta function  $\delta_{ij}$  is 1 for  $i = j$  and zero otherwise). In other words, there is no error in the off-diagonal elements of the susceptibility tensor. In this case, the diagonal elements are each overestimated by an amount  $\Delta M$ . An isotropic error of this sort leads to an overestimate of the mean value of  $k_p$ , an underestimate of the anisotropy of  $k_p$ , and no error in the orientations of the principal axes of  $k_p$ .

Alternatively, suppose that the ferromagnetic contribution to high-field slope varies with orientation. This situation may commonly arise in anisotropic samples whose ferromagnetic moments saturate quickly in their ‘easy’ direction(s) but approach saturation more gradually in the ‘hard’ direction(s) (Fig. C1). The result here would be errors  $\Delta\mathbf{M}_{\text{HF}}$  that tend to be negatively correlated with the low-field ferromagnetic susceptibilities  $\mathbf{M}_{\text{F}}$ , and consequently the estimated high-field anisotropy  $\mathbf{k}'_{\text{HF}}$  would be ‘contaminated’ by what would appear to be a component bearing an ‘inverse’ relationship to  $k_p$ . The mean  $k_p$  is overestimated in this situation. The errors, in this case, in principal axis magnitudes and orientations would depend on the relationship between the ferromagnetic and paramagnetic fabrics.

Systematic errors related to sample shape, heterogeneity and sample position, as discussed in Appendix A and in the text, are most significant when they have a component that varies as  $\sin(2\theta)$ . Such periodicities are mapped by  $\Delta\mathbf{k} = \mathbf{G}\Delta\mathbf{M}$  into apparent anisotropies. If measurements are made at  $45^\circ$  increments, as we do for HFAMS, periodic measurement errors are  $\Delta\mathbf{M} \propto \sin(n\theta r\phi)$ ,  $\Delta\mathbf{k} = 0$  for  $n = 1$  and  $n = 4$ . More limited sampling schemes do not suffice to eliminate these periodic errors. For example, when only 15 measurements

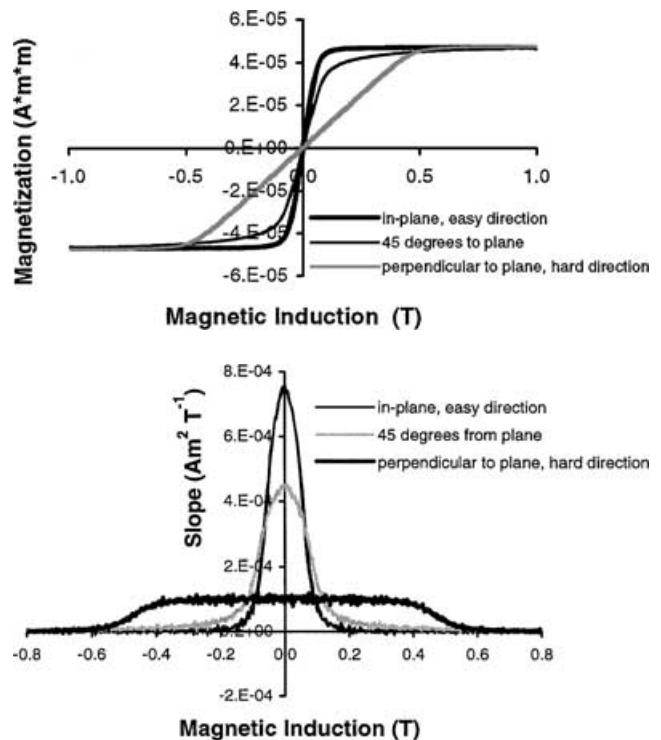


**Figure C1.** (a) Hysteresis loops for a piece of Nickel foil along the easy direction (along the plane of the foil), the hard direction (perpendicular to the plane of the foil) and at an intermediate direction (45 degrees to the plane of the foil). (b) The first derivative of the hysteresis loop from part A which is a measure of the DC susceptibility. The easy direction contributes most strongly to the low field susceptibility, while the hard direction contributes significantly to the high field susceptibility.

are made (as in the standard Kappa system), periodic errors with  $n = 1$  or  $n = 4$  may produce nonzero  $\Delta k_s$  (depending on their phase  $\phi$  with respect to the measurement set). Although such periodic errors do not commonly arise during low-field AMS measurements, they are important for our HFAMS technique. Therefore it is critical to collect data in all 24 orientations. (Note that reducing the 24 measurements to 15, by averaging axially equivalent data as we have done, also suffices to eliminate periodic errors with  $n = 1$  or  $n = 4$ ).

Overall, error minimization requires balancing the various types of error against one another. Sample shape effects are minimized when the magnet pole gap and coil spacing are large compared to the sample dimensions. However larger pole gaps also reduce the maximum available field, so that nonsaturation of ferromagnetic materials becomes a concern. For homogenous fine-grained samples, samples can be cut to smaller dimensions reduce both shape effects and nonsaturation. Heterogenous coarse-grained rocks are less suitable for the presented technique.